J Mater Sci (2010) 45:6030–6037
DOI 10.1007/s10853-010-4687-x

The effects of surface modification on the supercapacitive behaviors of carbon derived from calcium carbide

Liping Zheng · Ying Wang · Xianyou Wang · Xingyan Wang · Hongfang An · Lanhuan Yi

Received: 17 January 2010 / Accepted: 31 May 2010 / Published online: 30 June 2010

Abstract The capacitive behaviors of calcium-carbide-derived carbon (CCDC) before and after nitric acid (HNO_3) modification are investigated. The structure and morphology of the HNO_3-modified CCDC (M-CCDC) are examined by X-ray diffraction, scanning electron microscopy, and transmission electron microscopy. The performances of the supercapacitor using M-CCDC as electrode active material are studied by cyclic voltammetry, galvanostatic charge/discharge, electrochemical impedance spectroscopy, and cycle life measurements. The results show that the capacitance of the supercapacitor increases from 154.7 to 196.5 F g^{-1} and the capacitance decay is only 1.3% over 10,000 cycles for the M-CCDC, which exhibits higher capacitive performance than the pristine CCDC electrode in the aqueous electrolyte solution. The superiority of the M-CCDC in capacitance properties is caused by the variations of surface wettability and the interstitial pore structure of CCDC, which results from the introduction of polar oxygen functional groups onto the CCDC surface by HNO_3 modification.

Introduction

Electrochemical capacitors (EC), or supercapacitors, have played an increasingly important role in power source applications such as hybrid electric vehicles and short-term power sources for mobile electronic devices, due to their high power energy density and long cycle performance [1]. According to energy storage mechanism, there are two types of supercapacitors, viz., electrochemical double layer capacitors (EDLCs) and redox supercapacitors. EDLCs have emerged as a promising energy storage option for applications that need high power along with exceptional storage and cycle life [2]. In the EDLCs, energy storage arises mainly from the accumulation of electronic and ionic charges at the interface between the electrode materials and the electrolyte solution. Therefore, the large surface area and the porosity of electrode active materials are the basic requirements to achieve high specific capacitance. Carbon materials have been considered as good candidates for supercapacitors because of their high specific area, long cycle life, low cost, and wide use in aqueous and non-aqueous solvents [3, 4].

In comparison with the traditional porous carbon materials including activated carbons [5], carbon aerogels [6], templated carbons [7], and their mixture with metal oxides [8, 9], or polymers [10–12], a new group of porous carbon materials, carbide-derived carbons (CDCs), which have high specific surface area (SSA) and fine-tuned pore sizes, have been receiving attention in the literature for applications in EDLCs [13, 14]. However, it has been found that usual porous carbon materials have a lower capacitances than expected, which is primarily attributed to the pore size, carbon microstructure, surface functional groups and so on, especially the poor wettability of the micropores in electrolyte solutions [15], which results in a less accessible surface area for the formation of electric double-layer. To improve wettability and capacitance performance of carbon materials, chemical surface modification in acid solutions have been investigated [4, 16].

L. Zheng · X. Wang (✉) · X. Wang · H. An · L. Yi
School of Chemistry, Key Laboratory of Environmentally Friendly Chemistry and Applications of Minister of Education, Xiangtan University, Hunan 411105, People's Republic of China
e-mail: wxianyou@yahoo.com

Y. Wang
School of Chemical Engineering and Pharmacy, Wuhan Institute of Technology, Hubei 430073, China

In addition, poor wettability of electrode material brings about high resistance to the transport of electrolyte ions within micropores of porous carbon during charge/discharge processes, resulting in large energy consumption by supercapacitor itself [17]. Thus, the development of porous materials by increasing surface functional groups through chemical modification is an effective technique to improve the electrochemical performance of capacitors.

In our previous work [18], the nanostructured skeleton carbon with network structures was prepared by directly etching of calcium carbide in chlorine at low temperatures and used as the electrode active materials of supercapacitors. In order to further enhance the capacitance, in this article, we report surface chemical modification of CCDC with HNO_3 solution. The HNO_3-modified CCDC was used as electrode active materials for supercapacitors, and the supercapacitive characteristics were studied by cyclic voltammetry, galvanostatic charge/discharge, electrochemical impedance spectroscopy, and cycle life measurements, respectively.

Experimental

Material synthesis

Synthesis of CCDC

The precursor CaC_2 (formula weight 64.10 g mol^{-1}, density 2.22 g cm^{-3}) was obtained from Alfa Aesar. To etch Ca from CaC_2, CaC_2 powders were placed in a quartz tube furnace. The tube was Ar purged for 30 min, then heated to 400 °C. Once the desired reaction temperature was reached, fresh prepared chlorine gas was directly passed through the tube furnace for 2 h. After chlorination, the furnace was cooled down to room temperature under an Ar purge. The resultant product was soaked in HCl solution (3 mol L^{-1}) and then washed with distilled water to remove further remainder. Acidic product was washed into neutral condition and then dried in desiccator at 80 °C.

Modification of CCDC

The resultant CCDC sample was soaked in 6 mol L^{-1} HNO_3 solution at 70 °C for 4 h, then filtrated and washed with distilled water till the pH value of the filtrate reached 7. The resulting CCDC was dried in vacuum at 80 °C for 24 h, denoted as M-CCDC.

Measurement techniques for structural characterization

(1) The surface area and pore-volumes of carbon materials were calculated from nitrogen adsorption isotherms at 77 K (Quantachrome NovaWin2) using the Brunauer, Emmett, and Teller (BET), and Barrett, Joyner, and Halenda (BJH) methods, respectively.
(2) The morphology of CCDC and M-CCDC were observed using a scanning electron microscope (JSM-6700F).
(3) The transmission electron microscopy (TEM) examination was performed using a FEI Tecnai G2 microscope at 200 kV.
(4) The FTIR measurements of different samples were performed with a Fourier transform infrared (FTIR) spectrometer (Perkin-Elmer Spectrum one) in the wave number range from 4000 to 500 cm^{-1}, using the KBr disk method.

Preparation of electrode and coin supercapacitor assembly

The mass ratio of CCDC/graphite was 8:1. The powder mixture was mixed with 10 wt% of polytetrafluoroethylene (PTFE) aqueous suspension as a binder to obtain a paste. The paste was then pressed into the nickel foam substrate using a spatula. After drying in vacuum at 80 °C for 12 h, the electrode of nickel foam was pressed at 16 MPa for 1 min to assure a good electronic contact and to form a circular tablet (diameter = 1.4 cm).

Symmetrical coin supercapacitors were constructed, in which two CCDC or M-CCDC electrodes are separated by a separator of electrode/separator/electrode order. The supercapacitors were filled with 6 mol L^{-1} KOH electrolyte and then sealed with packing machine.

Electrochemical measurements

The electrochemical performances of the electrodes were characterized by cyclic voltammetry (CV) and electrochemical impedance test. The experiments were carried out using a three-electrode system, in which nickel foam and the saturated calomel electrode (SCE, 0.242 V versus the normal hydrogen electrode (NHE)) are used as counter and reference electrodes, respectively. The used electrolyte was 6 M KOH solution. The charge/discharge and the cycle life measurements at constant current were carried out by potentiostat/galvanostat on button cell supercapacitors.

Results and discussion

Structure and morphology

Usually, CDC prepared from carbide precursor in the literature involves complicated reaction mechanism and few

direct synthesis methods are reported. Our group has put forward one-step direct synthesizing CCDC process at 400 °C by chlorination of CaC_2, in which CaC_2 was chloridized by freshly prepared Cl_2 because the freshly prepared Cl_2 contained a lot of highly active chlorine-free radicals [18]. Figure 1 shows the typical adsorption/desorption isotherms of N_2 at 77 K and their pore size distributions for CCDC and M-CCDC. The results show that both isotherms (Fig. 1a) are the type IV, which is associated with the presence of mesopores. The hysteresis of M-CCDC widens presumably as a result of increased mesopore number, suggesting that the diffusion of carbon atoms increased and bigger pores obtained after HNO_3 activation. The porosity characteristics of CCDC and M-CCDC evaluated from the N_2 adsorption measurements are shown in Table 1. It shows that the BET surface area, average pore diameter, and mesopore volume of M-CCDC are higher than that of CCDC, which indicates preferable pore structure after HNO_3 activation.

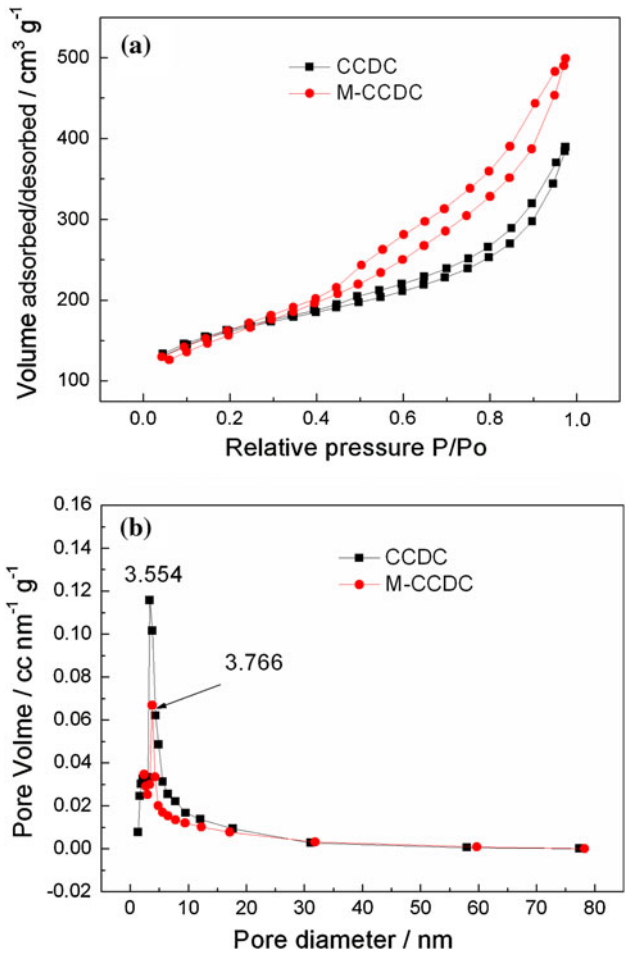

Fig. 1 Nitrogen adsorption isotherms at 77 K (**a**) and pore size distribution plots (**b**) of CCDC and M-CCDC

Figure 2 shows the powders X-ray diffraction (XRD) patterns of CCDC and M-CCDC. The XRD patterns reveal the broad characteristic peaks at $2\theta = 26°$, which correspond to diffraction from (002) planes of graphite. The broad peaks suggest a highly disordered and amorphous structure of the carbon material derived from CaC_2. It is found that the peak (002) of M-CCDC (curve b) becomes narrower, indicating the improved crystalline structures. The peak at $2\theta = 44°$ seems to be inconspicuous, indicating no graphitization tendency in CCDC.

The morphologies and microstructures of the CCDC were examined by scanning electron microscopy (SEM) and transmission electron microscope (TEM). Figure 3 shows SEM and TEM images of CCDC and M-CCDC. As shown in Fig. 3a, the as-prepared CCDC is consisted of agglomerated small framework. After modified by HNO_3 (Fig. 3b), the surface morphology of M-CCDC becomes salient and rough, indicating the increase of the surface area of M-CCDC. It is in good agreement with the result of BET test. TEM investigations could indeed reveal the highly porous character of CCDC materials. It can be found from Fig. 3c that the CCDC is completely amorphous carbon with no detectable graphite layers, and has small particle size less than 5 nm and no agglomerated morphology. As shown in Fig. 3d, the channels structure of M-CCDC becomes more obvious and the pore sizes are enlarged synchronously, which are beneficial to the transport of electrolyte ions within micropores of CCDC during charge/discharge processes, and to the formation of electric double layer.

FTIR spectra

FTIR analysis was performed to study the surface functional groups of the CCDC material modified by HNO_3. Figure 4 shows FTIR spectra of pure CCDC and M-CCDC. It can be clearly seen from curve (a) that characteristic peaks appear at 3444 and 1096 cm^{-1}, which are ascribed to

Table 1 Porosity characteristics of CCDC and M-CCDC evaluated from the N_2 adsorption measurements

Samples	A_{BET} (m^2 g^{-1})	d_{BJH} (nm)	V_{tot} (cm^3 $g^{-1)}$	V_{mi} (cm^3 g^{-1})	V_{me}/V_{tot} (%)
CCDC	612	3.554	0.629	0.028	95.2
M-CCDC	658	3.766	0.586	0.022	96.5

A_{BET} BET surface area, V_{mi} micropore volume, V_{tot} total volume, V_{me} mesopore volume, d_{BJH} average pore diameter

–OH (3500 cm^{-1}) and C–C–O (1096 cm^{-1}) stretching bands, respectively [19]. In curve b, the M-CCDC presents many characteristic peaks of oxygenous functional groups, which can be indexed in the range of 3150–1200 cm^{-1}. The characteristic peaks positioned at 1722.0, 1631.1, and 1406.2 cm^{-1}, correspond to –COOH, –CO–, and COO^- stretching vibration bands, respectively [20]. Therefore, chemical modification results in oxygenous functional groups on the surface of CCDC which increases the hydrophile performance of CCDC, and thus facilitates the formation of electric double-layer and improves the capacitance properties of the material. Besides, element analysis for CCDC and M-CCDC has also confirmed that the content of N and O increased to 2.15 and 3.6% from 1.95 and 3.0% for modified CCDC. It is further confirmed that the oxygenous functional groups are generated on the surface of M-CCDC after the modification.

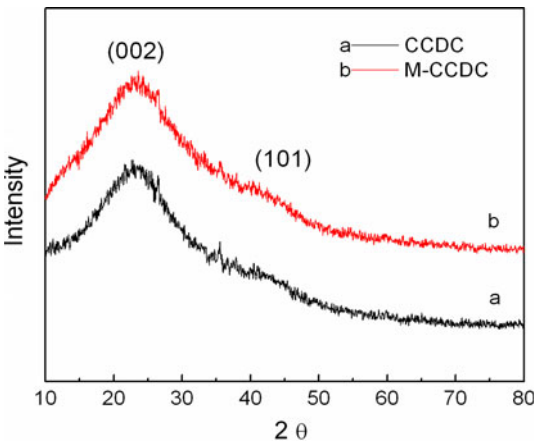

Fig. 2 The XRD patterns of CCDC and M-CCDC

Electrochemical properties

Cyclic voltammetry

Cyclic voltammetry is a useful tool to determine the faradaic and nonfaradaic behaviors and evaluate the capacitance of the electrode materials. Figure 5 shows cyclic voltammetries of the CCDC and M-CCDC as electrodes at various scan rates. The CV curves for both materials exhibit an approximately rectangular CV shape which indicates good capacitive behavior of CCDC and M-CCDC. The slight deviation from ideal rectangular shape is due to the resistance of the electrolyte and the contact resistance between the electrode and the current

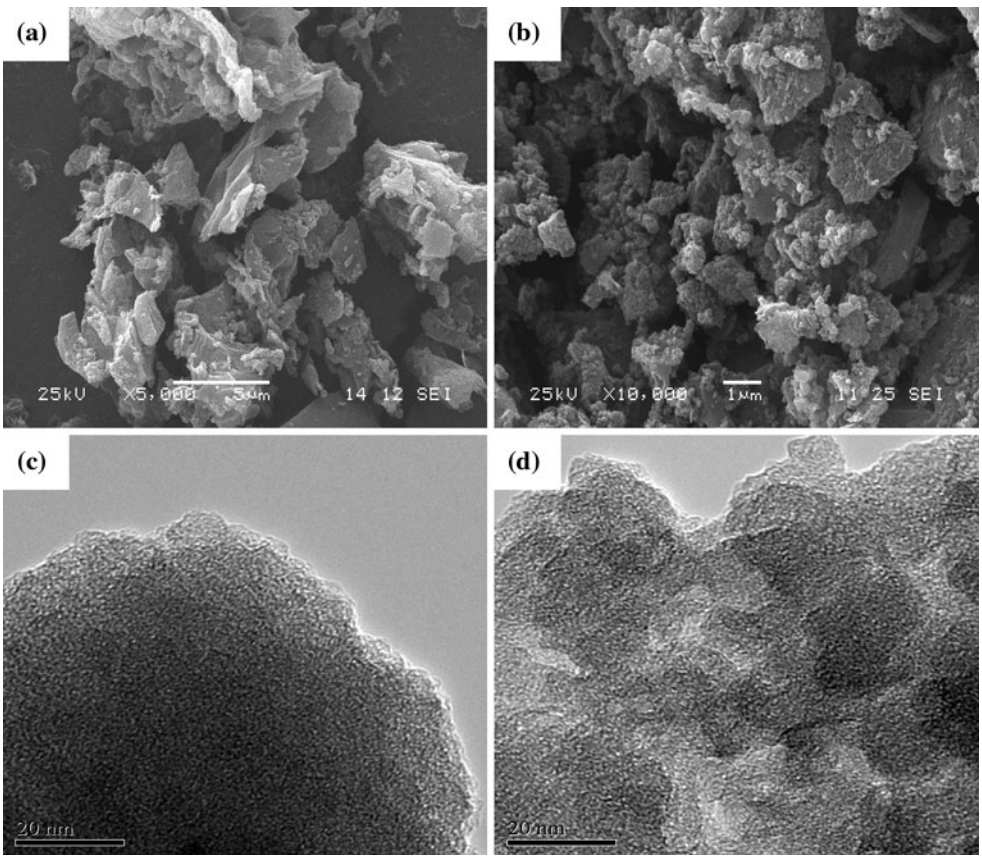

Fig. 3 SEM image of (**a**) CCDC and (**b**) M-CCDC; TEM image of (**c**) CCDC and (**d**) M-CCDC

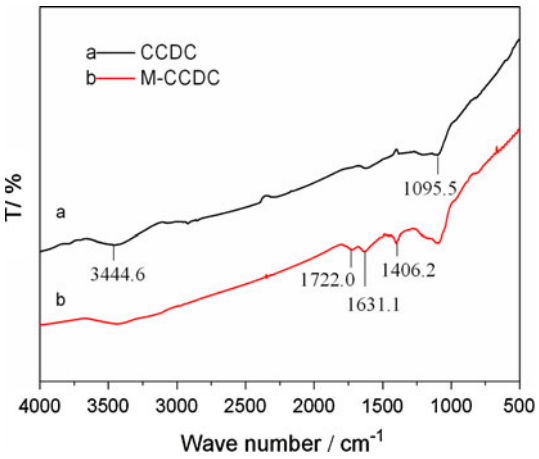

Fig. 4 FTIR spectra of (**a**) CCDC and (**b**) M-CCDC

collector. At the same scan rate, more ideal capacitive behavior was observed for the M-CCDC with a steeper current change at the switching potentials (0 and 1.0 V), resulting in higher capacitance. Note that a wide hump during the cathodic sweep can be clearly observed on the CV plot for M-CCDC (Fig. 5b), which is a signature of pseudocapacitance. It is evident that reversible redox transitions involving proton exchange occur when the samples are polarized [21]. However, in the case of CCDC, the pseudo-Faradic reactions can not be identified (Fig. 5a). In Fig. 5, whether CCDC or M-CCDC electrodes, the specific capacitance decreases with the increase of scan rate. At low scan rate, the ions have enough time to diffuse into the inner surface of channels and micropores of CCDC. Thus, the penetration distance and easily accessed pore channels play less important roles at such stage, while at high scan rate, the ions can only penetrate into the inner surface of relatively large pores, which indicates that less active surface area of the pores is taking part in the electrochemical processes [22].

A quantitative estimation of the capacitance can be obtained from the CV curves using Eq. 1 [23]:

$$C = \frac{I_a + |I_c|}{2m(dV/dt)} \quad (1)$$

where C is the specific capacitance of electrodes (F g^{-1}); I_a and I_c are the currents of anodic and the cathodic voltammetric curves on positive and negative sweeps, respectively; m is the mass of the CCDC (g) and dV/dt is the scan rate(V s^{-1}). Table 2 tabulates the specific capacitance of CCDC and the M-CCDC, which was measured based on three-electrode system and calculated according to Eq. 1. Comparing the data in Table 2, a higher specific capacitance can be obviously observed for M-CCDC. The specific capacitance value of CCDC at a scan rate of 1 mV s^{-1} increased from 154.7 to 196.5 F g^{-1} after the modification. In Table 2, although the specific capacitance decreases

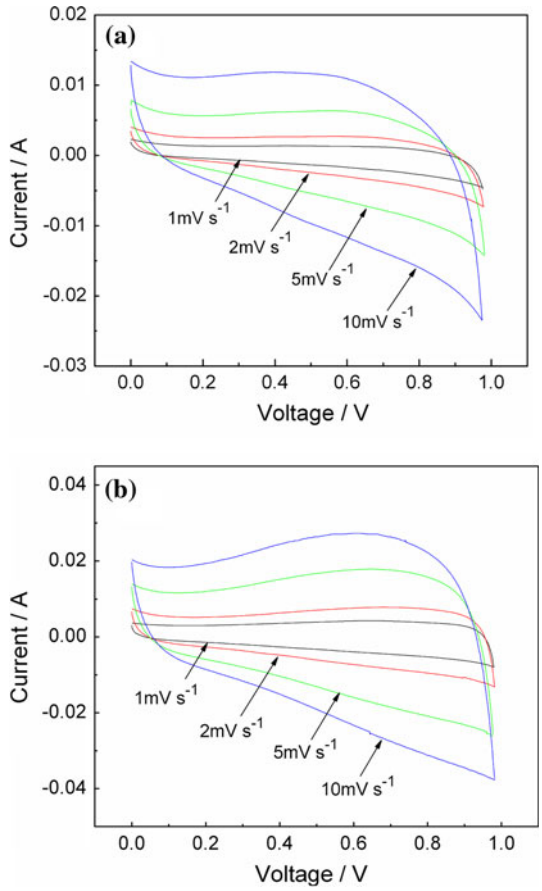

Fig. 5 Cyclic voltammograms for (**a**) CCDC and (**b**) M-CCDC electrodes at various scan rates

with the increase of scan rate, the specific capacitance for M-CCDC is clearly higher than that of CCDC at every given scan rate.

Electrochemical impedance spectroscopy

In order to better understand the electrochemical performances of CCDC and M-CCDC, the electrochemical impedance spectroscopies (EIS) are shown in Fig. 6. EIS measurements were conducted on the system at open voltage in a fully discharge stated at frequencies from 100 kHz to 10 mHz. The high-frequency arc is probably due to the charge transfer reaction and the inclined line in the low-frequency range is attributable to Warburg

Table 2 The specific capacitances of CCDC and M-CCDC elecrodes

Samples	Specific capacitance (F g^{-1})			
	1 (mV s^{-1})	2 (mV s^{-1})	5 (mV s^{-1})	10 (mV s^{-1})
CCDC	154.7	140.5	121.9	108.2
M-CCDC	196.5	184.3	170.7	155.1

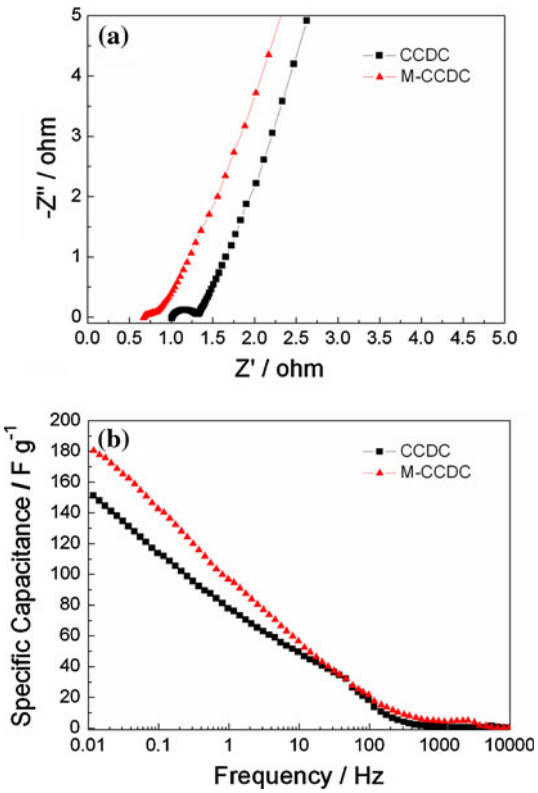

Fig. 6 Nyquist plots (**a**) and the changes of specific capacitance with frequency (**b**) of the CCDC and M-CCDC electrodes

impedance. The diameter of the semicircle for CCDC is clearly bigger than that of the M-CCDC in the high-frequency region (between 100 kHz and 400 Hz), which indicates lower electrochemical reaction resistance after the modification. As shown in Fig. 6a, the charge-transfer resistance is estimated to be 0.34 and 0.15 Ω from the diameter of the semicircles for CCDC and M-CCDC, respectively. A decrease of impedance, namely, decrease in the polarization resistance R, is primarily attributable to the improved wettability and the higher ionic conductivity of electrode material [24]. In the low-frequency regime, both CCDC and M-CCDC show approximately ideal capacitive behavior, with a near vertical line parallel to the imaginary axis.

Figure 6b presents the changes of the specific capacitance with frequency based on Fig. 6a. The specific capacitance was obtained from Eq. 2 [25]:

$$C = -\frac{1}{2\pi f m Z''} \tag{2}$$

Here, C is specific capacitance, f is the frequency, Z'' is imaginary part in impedance, and m is the weight of active materials. As seen in Fig. 6b, the specific capacitance gradually decreases with the increase of frequency for CCDC and M-CCDC but the specific capacitance values for M-CCDC is always higher than CCDC. The results are in good agreement with cyclic voltammetry experimental data.

Galvanostatic charge/discharge

The charge/discharge curves of M-CCDC electrodes measured at different current density within a potential window (0 to 1 V vs. SCE) are showed in Fig. 7a. As shown in Fig. 7a, discharge time increases distinctly with current density decreasing. The specific capacitance of M-CCDC electrodes can be calculated from Eq. 3 [9].

$$C = \frac{I \cdot t}{\Delta V \cdot m} \tag{3}$$

where C is the specific capacitance of coin (F g^{-1}), I is discharge current (A), t is the discharge time(s), m is the weight of active materials (g) and ΔV is 1 V.

In Fig. 7b, there are compared galvanostatic charge/discharge curves for the CCDC electrode and M-CCDC electrode at 0.5 A g^{-1}. The area surrounded by charge/discharge curves and x-coordinate is apparently increased after HNO_3 modification, indicating that the capacitance of M-CCDC is larger than that of the CCDC electrode. The

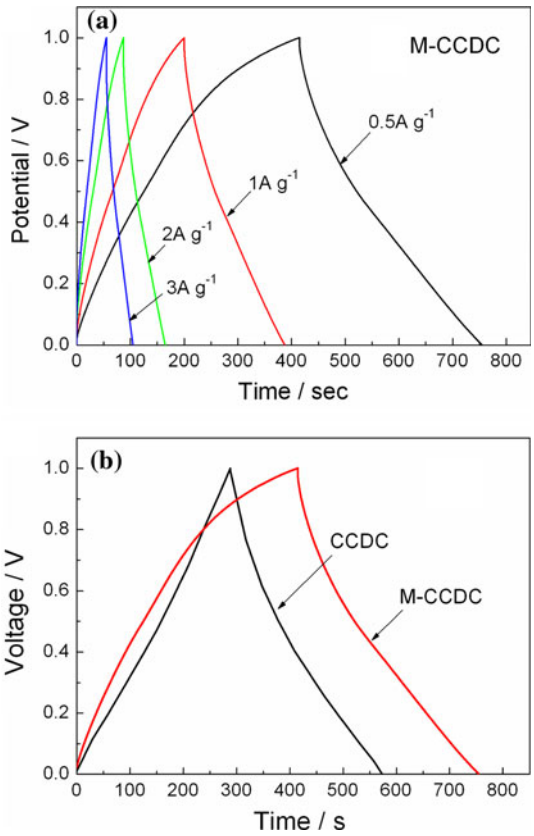

Fig. 7 Charge/discharge curves for (**a**) CCDC electrodes at different current density and (**b**) comparison of CCDC and M-CCDC at 0.5 A g^{-1}

reason may be that much more electrochemically active surface can be provided and electrolyte ions can occupy more pores within the electrode to participate in the formation of the electrochemical double-layer after activation. Comparing the shapes of the charge/discharge curves of CCDC and M-CCDC, it is clear that the potential of CCDC electrode varies nearly linearly with time, while the curves of M-CCDC deviate from ideal linear line, indicating that the specific capacitance of the M-CCDC electrode is consisted of electric double layer capacitance and Faradaic capacitance due to existence of containing O functional group in the surface.

Cycle life

The cycle life is an important factor for electrochemical capacitance performances of supercapacitors. As shown in Fig. 8, the specific capacitances of CCDC and M-CCDC are given as a function of cycle number. The test of cycle life was performed at a current density of 0.5 A g^{-1}. In Fig. 8, both supercapacitors have very long cycle life under shallow depths of discharge in the potential range of 0–1.0 V, but the capacitance of the supercapacitor using M-CCDC as electrode active material is apparently higher than the other. The capacity decays of CCDC and M-CCDC are 6.1 and 1.3% after 10,000 cycles, respectively, which indicates that the modified carbons possess excellent cycle stability. Such a low decrease in specific capacitance after the long charge/discharge cycle indicates the high stability of the activated CCDC and potential advantage as an electrode active material for long-term supercapacitor applications. In addition, it is also found that the difference in capacity decay between the CCDC and the M-CCDC is very small, which indicates that surface modification with HNO_3 does not degrade the cycle performance of the original carbons. Therefore, HNO_3

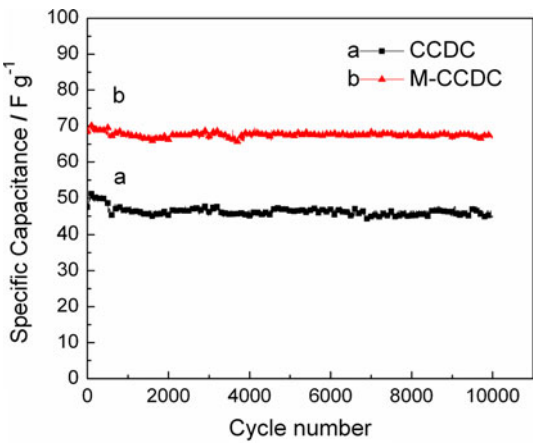

Fig. 8 Cycle life of the coin supercapacitors using (**a**) CCDC and (**b**) M-CCDC as electrode active materials

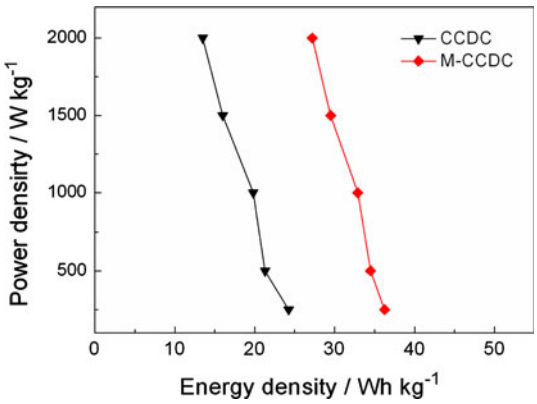

Fig. 9 Ragone plots of the CCDC and M-CCDC supercapacitors

activation treatment can not only promote the specific capacitance, but also improve the stability of CCDC and increase cycle life.

The excellent performance of CCDC and M-CCDC as the electrode material for supercapacitors can also be demonstrated in the Ragone plots. Figure 9 is the Ragone plot of the CCDC and M-CCDC supercapacitors. Energy density and power density are calculated using Eqs. 4 and 5 [26]:

$$E = \frac{1}{2}C(\Delta V)^2 \tag{4}$$

$$P = \frac{I\Delta V}{2m} \tag{5}$$

where C is the capacitance of the capacitors, I, ΔV, and m represent discharge current, range of the charge/discharge, the mass of active materials, respectively. Though the energy density of CCDC and M-CCDC decrease with the increase of power density, it can be apparently seen that the CCDC and M-CCDC supercapacitors achieved an energy density of 24.5 and 36.3 Wh kg^{-1}, respectively. In addition, the supercapacitors based on both the CCDC and the M-CCDC have an excellent power performance. However, with the increasing of the power density, the energy density of the CCDC supercapacitors decreases slightly faster than that of the M-CCDC supercapacitors because the speed of the side reactions from the impurity within CCDC is not as fast as the formation of the electric double-layer in the M-CCDC electrode. The enhancement in specific capacitance and energy density for M-CCDC is mainly attributable to improvement in wettability of CCDC, which results in a higher usable surface area and a smaller internal resistance.

Conclusion

The channel structures of CCDC modified by HNO_3 become more obvious and the pore sizes are enlarged

apparently. Activation treatment can introduce oxygenous functional groups on the surfaces of CCDC, which increases hydrophile performance of CCDC, and thus remarkably facilitates the formation of electric double-layer. The structure of CCDC remains unchanged after chemical modification by HNO_3, but the physical chemistry properties of CCDC are improved. It was found that the CCDC modificated by HNO_3 exhibited better electrochemical properties than the pure CCDC. The specific capacitance based on cyclic voltammetry increased from 154.7 to 196.5 F g^{-1} after the modification, and was scarcely changed after 10,000 charged/discharged cycles. Besides, the charge-transfer resistance decreased accordingly, suggesting lower electrochemical reaction resistance after the modification. It is confirmed that HNO_3 modification treatment can not only promote the specific capacitance, but also improve the stability of CCDC and increase cycle life. Therefore, surface modification treatment is an effective way to increase electrochemical performance of supercapacitors.

Acknowledgements This work was financially supported by the National Natural Science Foundation of China (Grant No. 20871101), Key Project of Education Department of Hunan Province Government (Grant No. 2009WK2007) and Fund for the Doctoral Program of Higher Education of China (Grant No.20943011100 Research 05).

References

1. Miller JR, Simon P (2008) Science 321:651
2. Miller JR, Burke AF (2008) Interface 17:44
3. Simon P, Gogotsi Y (2008) Nat Mater 7:845
4. Burke A (2007) Electrochim Acta 53:1083
5. Liu Y, Li KX, Wang JL, Sun GH, Sun CG (2009) J Mater Sci 44:4750. doi:10.1007/s10853-009-3710-6
6. Gutiérrez MC, Picó F, Rubio F, Amarilla JM, Palomares FJ, Ferrer ML, Monte FD, Rojo JM (2009) Mater J Chem 19:1236
7. Tiemann M (2008) Chem Mater 20:961
8. Kim Y-T, Tadai K, Mitani T (2005) J Mater Chem 15:4914
9. Huang QH, Wang XY, Li J (2006) Electrochim Acta 52:1758
10. Peng C, Zhang SW, Jewell D, Chen GZ (2008) Prog Nat Sci 18:777
11. Zhang H, Cao GP, Wang WK, Yuan K, Xu B, Zhang WF, Cheng J, Yang YS (2009) Electrochim Acta 54:1153
12. Tamai H, Hakoda M, Shiono T, Yasuda H (2007) J Mater Sci 42:1293. doi:10.1007/s10853-006-1059-7
13. Gogotsi Y, Welz S, Ersoy DA, McNallan MJ (2001) Nature 411:283
14. Largeot C, Portet C, Chmiola J, Taberna PL, Gogotsi Y, Simon P (2008) J Am Chem Soc 130:2730
15. Ma R, Liang J, Wei B, Zhang B, Xu C, Wu D (1999) J Power Sources 84:126
16. Hulicova-Jurcakova D, Puziy AM, Poddubnaya OI, Suárez-García F, Tascón JMD, Lu GQ (2009) J Am Chem Soc 131:5026
17. Simon P, Burke A (2008) Interface 17:38
18. Dai CL, Wang XY, Wang Y, Li N, Wei JL (2008) Mater Chem Phys 112:461
19. Wang YG, Li HQ, Xia YY (2006) Adv Mater 18:2619
20. Gheybi H, Bagheri M, Alizadeh Z, Entezami AA (2008) Polym Adv Technol 19:967
21. Béguin F, Ania CO, Khomenko V, Raymundo-Piñero E, Parra JB (2007) Adv Funct Mater 17:1828
22. Wang K, Wang Y, Wang Y, Hosono E, Zhou H (2009) J Phys Chem C 113:1093
23. Li J, Wang XY, Huang QH, Dai CL, Gamboa S, Sebastian PJ (2007) J Appl Electrochem 37:1129
24. Zhang J, Kong LB, Li H, Luo YC, Kang L J Mater Sci. doi: 10.1007/s10853-009-4186-0
25. Taberna PL, Portet C, Simon P (2006) Appl Phys A 82:639
26. Xue Y, Chen Y, Zhang ML (2008) Mater Lett 62:3884